Gigahertz laser ablation of lithium nickel manganese cobalt oxide for lithium-ion batteries

N. Straßburger*, P. Zhu, W. Pfleging
Karlsruhe Institute of Technology, IAM-AWP, P.O. Box 3640, 76021 Karlsruhe, Germany

ABSTRACT

Extensive technological progress is essential to meet the ambitious future requirements of energy storage devices. This is due to the necessity of achieving high energy and power density operations, accompanied by high safety standards and extended lifespans, while maintaining low production and material costs. Lithium-ion batteries (LIBs) are expected to continue to be the most preferred energy storage technology for the next decade. Significant importance is placed on the research of high energy active materials for optimizing this technology. However, besides material optimization, there is substantial potential for optimization by introducing electrodes with high mass loading, advanced electrode architecture, and their transfer to mass production and high technology readiness level. Achieving appropriate trade-offs between high energy and power density, process reliability, and economic considerations poses a challenge for current LIBs technology.

For this purpose, the laser-assisted generation of three-dimensional (3D) electrode architectures is studied and evaluated with respect to its impact on battery performances and a possible transfer to battery production. Advanced electrode design incorporates micro and sub-micron structures that can be designed in various ways. Significant improvements in battery lifespan and high power operation capabilities can be achieved compared to traditional two-dimensional (2D) electrodes. Ablation using high power ultrafast laser has proven to be a precise method for introducing such structures.

The production of 3D electrodes with laser support requires coordination with other established manufacturing steps in the battery production process. In particular, the calendering of electrodes holds great importance as it has a significant impact on the microstructural properties of the electrode material, including porosity, material density, and layer adhesion. The present study investigated the impact of laser-induced hierarchical structuring using GHz bursts, comprising micro-/nano-porosities and microtopography, on electrodes with an areal capacity of approx. 4.2 mAh/cm² and different porosity levels. In this regard, electrodes comprising $LiNi_{0.8}Mn_{0.2}Co_{0.2}O_2$ (NMC 811) were prepared, calendered to calculated porosities between 10% and 40% and subjected to materialographic characterization techniques.

Keywords: 3D battery, ultrafast laser structuring, calendering, electrodes, lithium nickel manganese cobalt oxide

1. INTRODUCTION

To meet evolving energy storage demands, continuous advancements in battery technology are required. LIBs have established themselves as the dominant energy storage solution due to their superior energy and power density, making them particularly suitable for applications such as electric vehicles (EVs). The need to further enhance LIBs technology has driven research into high energy active materials, thick-film electrodes, and novel electrode architectures [1].

High energy electrode materials, combined with thick-film electrodes exceeding 100 µm in film thickness, have enabled commercial LIBs to achieve energy densities of up to 550 Wh/l. This translates to battery-electric vehicles (BEVs) achieving driving ranges of up to 500 km, which is comparable to those of internal combustion engine vehicles. However, challenges persist in optimizing the trade-off between energy density, power output, manufacturing reliability, and cost-effectiveness [2-4].

Beyond material development, further optimization can be achieved through advanced electrode design. Increasing electrode mass loading, integrating 3D electrode structures, and transferring these advancements to large-scale production are key strategies for improving future LIBs performance. Laser-assisted structuring has emerged as a viable approach, introducing micro- and sub-micron modifications that enhance the battery performance. Various structured designs, including line, grid, and hole patterns, have been shown to mitigate mechanical degradation, improve electrolyte wettability, enhance charge transport, and reduce lithium plating risks. High power ultrafast laser ablation is a precise and effective technique for fabricating such structures, but its integration with traditional battery manufacturing processes remains an important consideration [5-9].

One crucial step in LIB production is calendering, which significantly affects the microstructural characteristics of the electrode material, including porosity, electronic conductivity, density, wettability, and layer adhesion. Understanding the interplay between laser structuring and calendering is essential for optimizing LIB electrodes and refining the 3D battery concept. This study investigates the effects of GHz burst laser structuring on calendered $LiNi_{0.8}Mn_{0.2}Co_{0.2}O_2$ (NMC 811) electrodes, with porosities ranging from 10 to 40% [10-12].

2. EXPERIMENTAL

2.1 Electrode manufacturing

NMC 811-based electrodes were prepared by mixing NMC 811 powder (Gelon, China) with conductive carbon additives, including carbon black (C-nergy Super C65, Imerys G&C, Switzerland) and graphite (KS6L), using a polyvinylidene fluoride (PVDF, Solef® 5130, Solvay Specialty Polymers, France) binder dissolved in N-methyl-2-pyrrolidone (NMP, Merck KGaA, Germany). Table 1 shows the corresponding weight percentages of the aforementioned materials. The binder solution was prepared at a weight ratio of 1:10 (PVDF:NMP) and homogenized in a centrifugal mixer (SpeedMixer DAC 150 SP, Hauschild & Co., Germany). The slurry was coated onto aluminum foil (20 µm thickness) using a doctor blade and dried at 90°C for 2 hours. The resulting electrode sheets measured 80 x 240 mm², with an initial uncalendered film thickness of 97.9 ± 1.0 µm.

Table 1: Material and mass fraction of each component in the NMC 811 slurry.

Material	Mass fraction [wt.%]
NMC 811	92
Carbon black (SC65)	3
Conductive graphite (KS6L)	2
PVDF binder	3

The NMC 811 electrodes were subsequently calendered at 50°C using a precision rolling press (HR01, MTI Corporation, USA) to achieve target porosities ranging from 10% to 40%. Film thicknesses were measured using a digital gauge (Millimess 2000W, Mahr, Germany) for five measuring points in width and three in length to ensure consistency.

2.2 Laser structuring

The laser structuring experiments utilized a high-power GHz burst laser system (PXpv, EdgeWave GmbH, Germany) integrated into a laser micromachining system (MSV203 Laser Patterning Tool, M-SOLV LTD, UK). The laser operated at a wavelength of 1064 nm, with a maximum average power of 450 W, a pulse duration of 10 ps, and a repetition rate of 1 MHz. Line patterns were structured using laser power levels ranging from 10 to 100 W, a scanning speed of 20 m/s, a pulse spacing of 20 µm, and a fixed amount of three scan passes. With the variation of the laser power, multiple fluence levels were explored to determine optimal ablation conditions for slightly and strongly calendered electrodes with the corresponding high and low porosities. The burst fluence F_{Burst} $\left[\frac{J}{cm^2}\right]$ can be calculated using equation (1) and the results found in Table 2.

$$F_{Burst} = \frac{2 \cdot P_{avg}}{f_{rep} \cdot {\omega_0}^2 \cdot \pi} \quad (1)$$

With the average laser power P_{avg} $[W]$, repetition rate f_{rep} $[Hz]$, and beam waist ω_0 $[cm]$.

In addition to the varied laser power, the burst lengths were set to 50 and 500 ns. This implies a change of pulses from 50 to 500 in a single burst to be able to analyze the corresponding influence on the ablation behavior of NMC 811 electrodes.

Table 2: Used laser power range and resulting burst fluences.

Laser power [W]	Burst fluence [J/cm^2]
10	5.1
20	10.1
40	20.2
60	30.3
80	40.4
100	50.5

3. RESULTS AND DISCUSSION

3.1 Electrode manufacturing

Table 3 presents detailed parameters related to the film thickness and achieved porosity of the NMC 811 electrodes used in this study. For each porosity, the table delineates the variations in film thickness and correlates these measurements with the respective porosities achieved through the calendering process. For the purpose of better distinction, the porosities 28% and 18% are later referred to as their rounded values 30% and 20%.

Table 3: Achieved film thicknesses and porosities of the NMC 811 electrodes after calendering.

Calendered film thickness [µm]	Achieved porosity [%]
87.5 ± 0.9	40
72.9 ± 0.4	28 (30)
64.4 ± 0.7	19 (20)
58.5 ± 0.5	10

In addition to the film thickness measurement, the electrodes were examined using an optical microscope (MeF3A, Reichert Jung, Leica Microsystems GmbH, Germany). Figure 1 shows a decrease in film thickness as well as a reduction of the pore sizes of the NMC 811 electrodes.

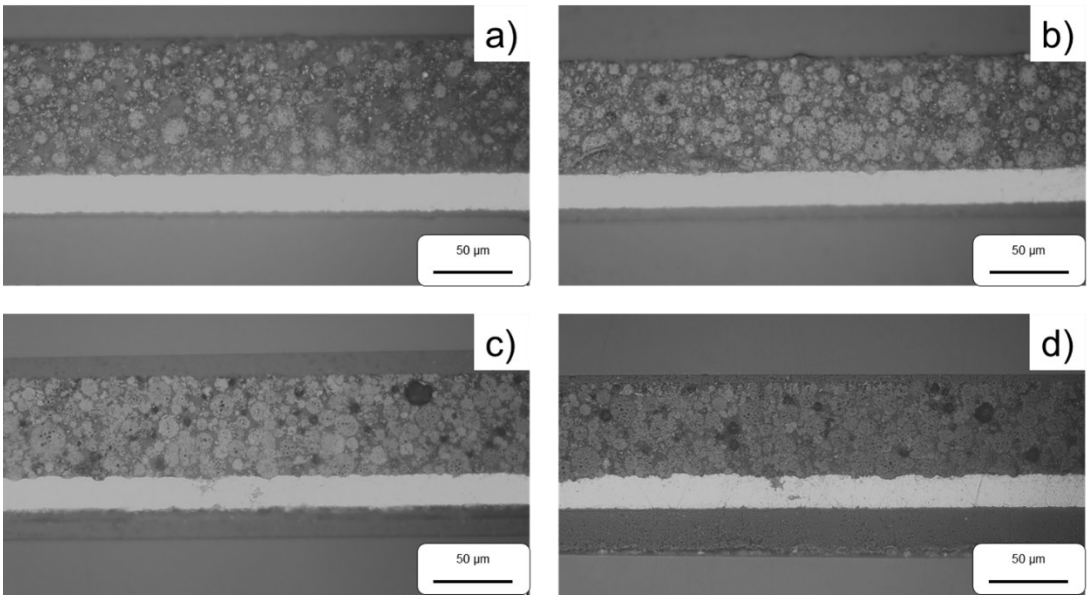

Figure 1: Cross sectional views of NMC 811 electrodes. Each image shows a different film thickness and porosity of 40% and 30% (represented in a and b) as well as 20% and 10% porosity (represented in c and d).

3.2 Laser structuring

Figure 2 shows the ablated area (cross section) versus the corresponding burst fluence. The data points in blue and green present the ablation of the high porosity electrodes with 40% and 30%, while the low porosity electrodes are displayed in yellow and red for 20% and 10%. Additionally, the 50 ns results are shown with squares and full lines, while the 500 ns results have triangles and dotted lines. This design scheme is also used in the fallowing graphs. At higher porosities the trend of shorter bursts ablating more area is shown, while at lower porosities that changes to longer bursts.

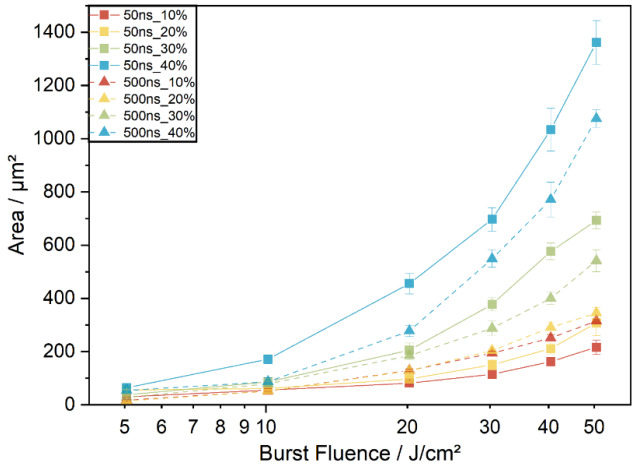

Figure 2: Ablated Area A as function of burst fluence F_{Burst} with values for 50 (square) and 500 (triangle) ns burst length as well as 40% (blue), 30% (green), 20% (yellow) and 10% (red) porosity.

As an addition to the before introduced ablated area, the ablation efficiency Eff $[\frac{mm^3}{J}]$ gets introduced with equation (2).

$$Eff = \frac{A \cdot v_{scan}}{P_{avg} \cdot n_{scan}} \tag{2}$$

This calculation allows for the evaluation of the ablated area A [µm²], scan velocity v_{scan} $[\frac{m}{s}]$, average laser power P_{avg} $[W]$, and number of repetitions n_{scan} $[-]$.

Figure 3 presents the ablation efficiency versus the used burst fluence. Here similar trends as in Figure 2 are shown with shorter bursts ablating material more efficiently at higher porosities, while longer bursts increase the efficiency at lower porosities.

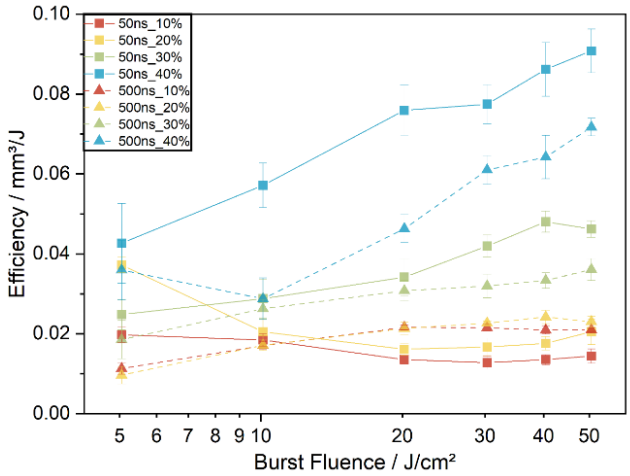

Figure 3: Ablation Efficiency Eff as function of burst fluence F_{Burst} with values for 50 (square) and 500 (triangle) ns burst length as well as 40% (blue), 30% (green), 20% (yellow) and 10% (red) porosity.

While the efficiency value is a useful indicator for upscaling, structures with optimal geometries, i.e. high aspect ratios are the focus. These structures or cavities reach to the current collector while remaining as narrow as possible. This helps to not waste unnecessary amounts of active material, which would also reduce the capacity unnecessarily. For this purpose, the aspect ratio AR [−] will now be considered and calculated with equation (3) by h [µm] defining the height and w_{FWHM} [µm] the full width at half maximum.

$$AR = \frac{h}{w_{FWHM}} \tag{3}$$

This aspect ratio value is now shown in Figure 4 and a clear trend for longer bursts achieving higher aspect ratios is recognizable for all porosities.

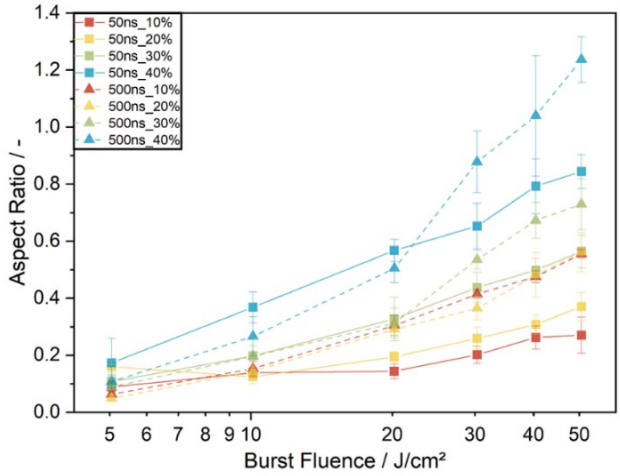

Figure 4: Aspect ratio AR as function of burst fluence F_{Burst} with values for 50 (square) and 500 (triangle) ns burst length as well as 40% (blue), 30% (green), 20% (yellow) and 10% (red) porosity.

To understand the ablation behavior and the aspect ratio further, the influences of both underlying parameters are analyzed in the following, h and w_{FWHM}. Starting with h in Figure 5, a similar ablation for lower and higher porosities as well as with shorter and longer bursts is shown.

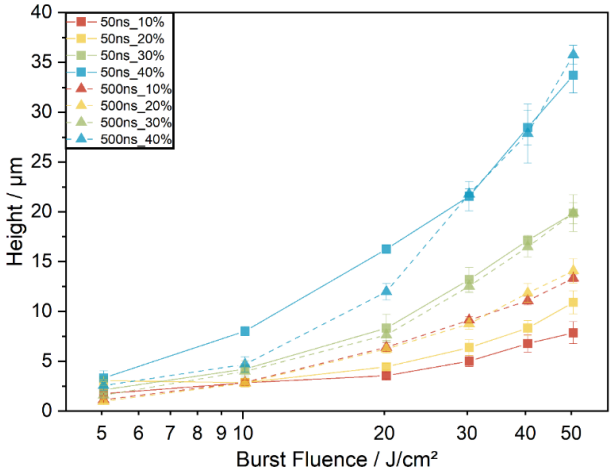

Figure 5: Ablated height h as function of burst fluence F_{Burst} with values for 50 (square) and 500 (triangle) ns burst length as well as 40% (blue), 30% (green), 20% (yellow) and 10% (red) porosity.

Additionally, w_{FWHM} is shown in Figure 6, which also presents a clear trend of longer bursts leading to lower ablated widths and clarifies that the trend of the aspect ratio is caused by the contribution of the ablated width.

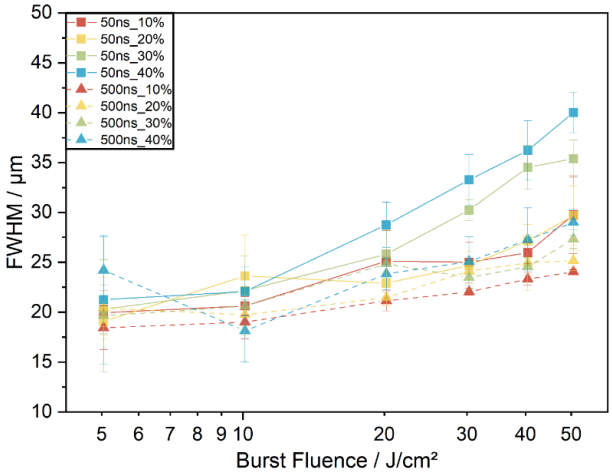

Figure 6: Ablated width w_{FWHM} as function of burst fluence F_{Burst} with values for 50 (square) and 500 (triangle) ns burst length as well as 40% (blue), 30% (green), 20% (yellow) and 10% (red) porosity.

4. CONCLUSION

The 3D battery concept and laser ablation with GHz bursts are promising technologies to further enhance LIBs. This work has demonstrated an ablation study with different burst fluences and burst lengths using GHz bursts for NMC 811 electrodes. Distinct ablation characteristics were identified based on porosity and burst length, revealing trends for the interplay between both parameters. Longer bursts resulted in improved structure geometries, as indicated by the aspect ratio, with similar height but reduced width. By optimizing the interplay of laser structuring and calendering, LIBs can be refined for specific use cases, for example to achieve high volumetric energy and power densities. Future work will explore higher burst fluences, additional burst lengths and repetition rates, as well as other binder systems. Additionally, the potential influence on material level, such as temperature related effects, will be analyzed and electrochemical analyses will be performed.

ACKNOWLEDGEMENTS

We are grateful to our colleagues Alexandra Reif and Heino Besser for their support during laser processing and analytics. This research has received funding from the European Union's Horizon Europe Research and innovation programme under Grant Agreement no. 101069705.

REFERENCES

[1] Bashir, T., Ismail, S.A., Song, Y., Irfan, R.M., Yang, S., Zhou, S., Zhao, J., Gao, L., 2022. A review of the energy storage aspects of chemical elements for lithium-ion based batteries. Energy Materials 1, https://doi.org/10.20517/energymater.2021.20

[2] Link, S., Neef, C., Wicke, T., 2023. Trends in Automotive Battery Cell Design: A Statistical Analysis of Empirical Data. Batteries 9, https://doi.org/10.3390/batteries9050261

[3] Shi, X., Pan, J., Wang, H., et al., 2019. Battery electric vehicles: What is the minimum range required?, Energy, https://doi.org/10.1016/j.energy.2018.10.056

[4] Ntombela, M., Musasa, K., Moloi, K., 2023. A Comprehensive Review for Battery Electric Vehicles (BEV) Drive Circuits Technology, Operations, and Challenges. World Electric Vehicle Journal 14, https://doi.org/10.3390/wevj14070195

[5] Chen, K.-H., Namkoong, M. J., Goel, V., et al., 2020. Efficient fast-charging of lithium-ion batteries enabled by laser-patterned three-dimensional graphite anode architectures, Journal of Power Sources, https://doi.org/10.1016/j.jpowsour.2020.228475

[6] Pfleging, W., 2022 - 2022. 3D electrode architectures for high energy and high power lithium-ion batteries. In: Balaya, P. et al. [Editors] Energy Harvesting and Storage: Materials, Devices, and Applications XII. SPIE. 2, https://doi.org/10.1117/12.2623655

[7] Pfleging, W., 2020. Recent progress in laser texturing of battery materials: a review of tuning electrochemical performances, related material development, and prospects for large-scale manufacturing. International Journal of Extreme Manufacturing 3, https://doi.org/10.1088/2631-7990/abca84

[8] Song, Z., Zhu, P., Pfleging, W., Sun, J., 2021. Electrochemical Performance of Thick-Film Li(Ni0.6Mn0.2Co0.2)O2 Cathode with Hierarchic Structures and Laser Ablation. Nanomaterials 11, https://doi.org/10.3390/nano11112962

[9] Jan Bernd Habedank. 2021. Laser Structuring of Graphite Anodes for Functionally Enhanced Lithium-Ion Batteries. Dissertation. München

[10] Primo, Emiliano N.; Chouchane, Mehdi; Touzin, Matthieu; Vazquez, Patricia; Franco, Alejandro A., 2021. Understanding the calendering processability of Li(Ni0.33Mn0.33Co0.33)O2-based cathodes. In: Journal of Power Sources 488, https://doi.org/10.1016/j.jpowsour.2020.229361

[11] Zheng, Honghe; Tan, Li; Liu, Gao; Song, Xiangyun; Battaglia, Vincent S., 2012. Calendering effects on the physical and electrochemical properties of Li[Ni1/3Mn1/3Co1/3]O2 cathode. In: Journal of Power Sources 208, https://doi.org/10.1016/j.jpowsour.2012.02.001.

[12] Sheng, Y., Fell, C.R., Son, Y.K., Metz, B.M., Jiang, J., Church, B.C., 2014. Effect of Calendering on Electrode Wettability in Lithium-Ion Batteries. Frontiers in Energy Research 2, https://doi.org/10.3389/fenrg.2014.00056